

RowDetr: End-to-End Row Detection Using Polynomials.

Rahul Harsha Cheppally

Department of Biology and Agricultural Engineering
Kansas State University United States
r4hul@ksu.edu

Ajay Sharda

Department of Biology and Agricultural Engineering
Kansas State University United States
asharda@ksu.edu

Abstract: Crop row detection has garnered significant interest due to its critical role in enabling navigation in GPS-denied environments, such as under-canopy agricultural settings. To address this challenge, we propose RowDetr, an end-to-end neural network that utilizes smooth polynomial functions to delineate crop boundaries in image space. A novel energy-based loss function, PolyOptLoss, is introduced to enhance learning robustness, even with noisy labels. The proposed model demonstrates a 3% improvement over Agronav in key performance metrics while being six times faster, making it well-suited for real-time applications. Additionally, metrics from lane detection studies were adapted to comprehensively evaluate the system, showcasing its accuracy and adaptability in various scenarios.

Keywords: Machine vision, Autonomous navigation, Crop row detection, Attention mechanism

1 Introduction

The application of autonomous robots in high-throughput phenotyping has experienced a significant surge in recent years, driven by the need for precision and efficiency in agricultural tasks [1]. These advanced robotic systems are transforming the field by automating the complex task of phenotyping with unparalleled accuracy. While autonomous solutions in agriculture have been explored for decades [2], recent advancements have pushed the boundaries of this technology, particularly in addressing challenges related to GPS-denied navigation in dense crop environments.

For nearly two decades, GPS-based autonomy has been the cornerstone of agricultural robotics. Studies such as [3] and [4] have showcased the use of RTK and GPS-based systems to guide tractors and harvesters with high precision. The GPS coordinates of rows can either be determined during planting or estimated using systems like [5, 6], which provide accurate crop and row location data. However, these GPS-based technologies face critical limitations under dense canopy cover, where GPS multi-pathing errors or complete signal loss render them unreliable. For example, the RoboBotanist project highlighted these challenges, encountering significant navigation difficulties beneath dense canopies due to GPS interference from leaf coverage [7]. These challenges emphasize the need for alternative solutions designed specifically for under-canopy navigation, where GPS-based methods fall short.

To overcome these limitations, researchers have explored vision-based strategies that do not rely on GPS. For instance, [8] utilized object detection to identify plants and employed visual odometry with fast features to estimate frame-to-frame transformations. Similarly, [9] introduced a method

combining a Kalman filter with neural networks to predict a robot’s orientation and position relative to crop rows. This method, integrated with sensor data in a moving horizon estimator, aimed to enhance navigation accuracy. However, these approaches struggled in scenarios with discontinuous crop rows or curved row structures, as noted in [10].

Further developments include an end-to-end detection network by [11], which predicts line segments for rows. While effective for straight rows, this method lacks the ability to handle curved rows due to its linear representation. Similarly, [12] applied YOLO and bounding box extraction for boundary detection, achieving a latency of 25ms but requiring additional post-processing steps. Segmentation-based methods, such as those proposed by [13, 14], rely on fully segmenting the image for row detection, achieving frame rates between 15 and 17 fps. However, their real-time applicability is constrained by computational inefficiencies, especially in densely foliated environments. While these methods address aspects of row navigation, their limitations persist in handling curved rows and dense canopy conditions.

In contrast, autonomous driving research has extensively explored lane detection, particularly methods leveraging polynomial regression for real-time performance. Techniques such as those proposed by [15, 16, 17] efficiently model lanes as polynomial functions, achieving lower latency compared to segmentation-based methods. Inspired by these advancements, this study proposes a novel under-canopy row detection framework, adapting polynomial modeling to agricultural row navigation. This approach leverages polynomials to provide smoother and more accurate row predictions, even in challenging scenarios.

Contributions

This study introduces several key contributions to the field of under-canopy row detection:

- A comprehensive dataset of 6,962 meticulously labeled images of sorghum and corn fields under canopy, curated specifically for under-canopy navigation tasks.
- A novel method for representing curves in an image, detailed in Section 2.2.1, enabling robust modeling of rows in diverse orientations.
- A custom loss metric, *PolyOptLoss* (Equation 4), which extends polynomial regression techniques from lane detection by incorporating geometric information. This energy-based loss enhances alignment accuracy, particularly when dealing with noisy labels.
- A custom model architecture, detailed in Section 2.3.2, designed for low-latency detection of dense and curved rows. The architecture achieves significant improvements in prediction accuracy and computational efficiency compared to existing frameworks such as Agronav [18].

These contributions collectively address the limitations of existing row navigation methods, advancing the capabilities of autonomous systems to navigate under dense canopy conditions or in GPS-denied environments with high precision and minimal latency. The subsequent sections provide a detailed explanation of the proposed methodology, dataset, and evaluation results, demonstrating the superiority of the proposed framework over existing methods in various row detection scenarios.

2 Methodology

This study is divided into two parts to evaluate the effectiveness of loss functions and model architecture for row detection. The first part investigates the impact of two distinct loss functions—Polynomial Regression Loss, as introduced in [16], and the proposed *PolyOptLoss*—on row detection accuracy and object proposals. The second part introduces a novel architecture for Row Detection using a complex encoder-decoder approach inspired by RtDetr [19], but employs polynomial proposals instead of traditional bounding box proposals with novel poly-sampler and offset layers.

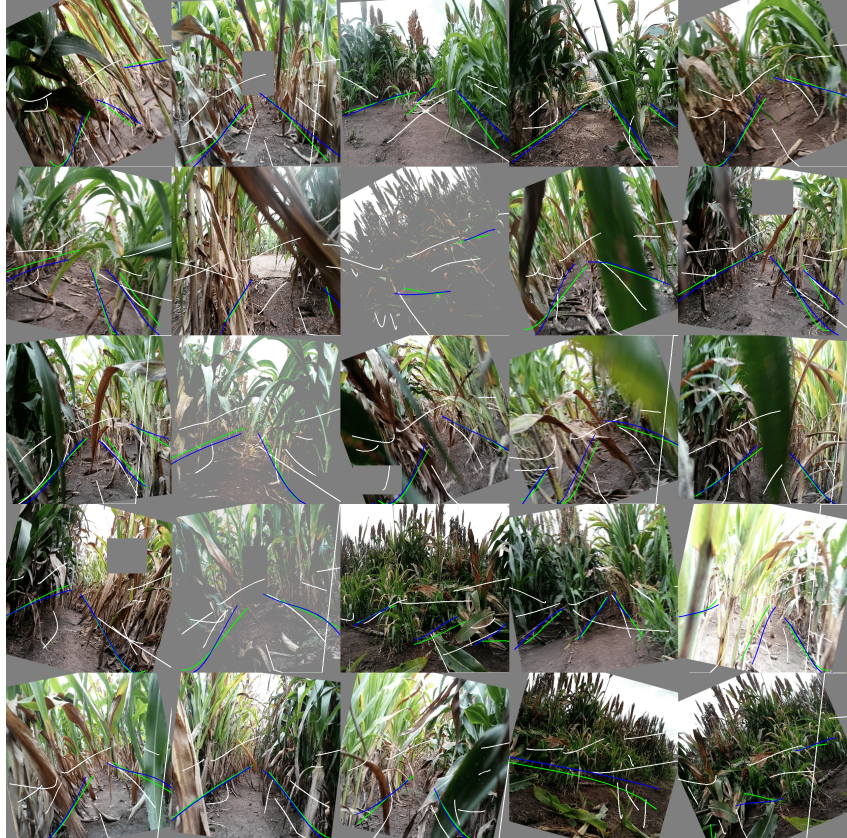


Figure 1: Samples from the training dataset: labeled samples (Blue), positive predictions with confidence greater than 0.5 (Green), and non-existent row predictions with confidence less than 0.5 (White).

2.1 Dataset

The dataset used for training the RowDetr Networks consists of multiple subsets collected under various conditions and using different devices, enhancing the diversity of scenarios. Figure 3 shows the distribution of images across each subset. Detailed data collection techniques are described below.

2.1.1 Robot Description

The under-canopy robot, depicted in Figure 2, was specifically designed to navigate the unique challenges of dense agricultural environments. It is equipped with a Jetson Orin [20] for onboard computation, providing the robust processing power required for real-time image analysis and decision-making. Actuator communication is managed through the Controller Area Network (CAN) protocol, ensuring reliable and efficient operation.

For image acquisition, the robot utilizes a Luxonis OAK-D Pro depth camera [21], known for its advanced vision processing capabilities. However, the performance of the depth camera is constrained under dense canopy conditions. Due to its baseline, the camera requires a minimum distance of 30 cm to generate accurate depth images. Given the narrow spacing between rows, typically around 75 cm, and the robot's track width of 55 cm, there is limited maneuverability, and the depth data becomes unreliable near the robot. To overcome these limitations, the RGB images from the camera were predominantly used for training the neural network, bypassing the constraints of depth imaging in such environments.



Figure 2: The under-the-canopy robot equipped with Jetson Orin and Luxonis OAK-D Pro for image acquisition.

The robot’s software is built on ROS2 [22], a robust and flexible framework that supports the development of complex robotic systems. ROS2 enables seamless communication between various software components using a publisher-subscriber model, facilitating efficient data handling and processing.

For mobility, the robot employs a skid-steer drive system, which is particularly well-suited for environments requiring low-radius turns, such as when exiting rows. This drive system balances the need for maneuverability with simplicity in control, making it ideal for operation under dense canopy conditions.

2.1.2 Dataset Collection

Corn V5 (1250 images): This subset was collected during a 45-minute session using handheld devices, including Samsung Galaxy and iPhones. Controlled variations were introduced by applying manual disturbances to the handheld device. To reduce spatial redundancy, a single frame was selected every 2.16 seconds, resulting in a total of 1250 unique images.

Corn V4 and Corn V6 (835 and 795 images, respectively): These datasets were captured using a metering stick equipped with a Basler camera, as shown in Figure 4. The camera recorded at 3 FPS, and manual disturbances were introduced by shaking the stick to simulate realistic motion conditions. Images were initially saved as TIFF files and later converted to JPEG format for training purposes.

CRDL Dataset (1250 training images, 430 testing images, 250 validation images): Sourced from [14], this dataset was captured using a RealSense D435i RGB-D camera. Only the RGB channels were retained, as the objective was row detection in standard visual data. Images were annotated following the labeling methods described in Section 2.1.3.

Sorghum Dataset (2152 images): This dataset was collected through multiple ROS bags recorded during manual operation of the robot, as illustrated in Figure 2, while navigating beneath a sorghum canopy with plants at the harvest-ready stage. To limit spatial redundancy, every 25th frame (approximately 0.8 seconds apart) was selected, resulting in a total of 2152 unique images.

Row Detection Image Data Distribution by Collection Device

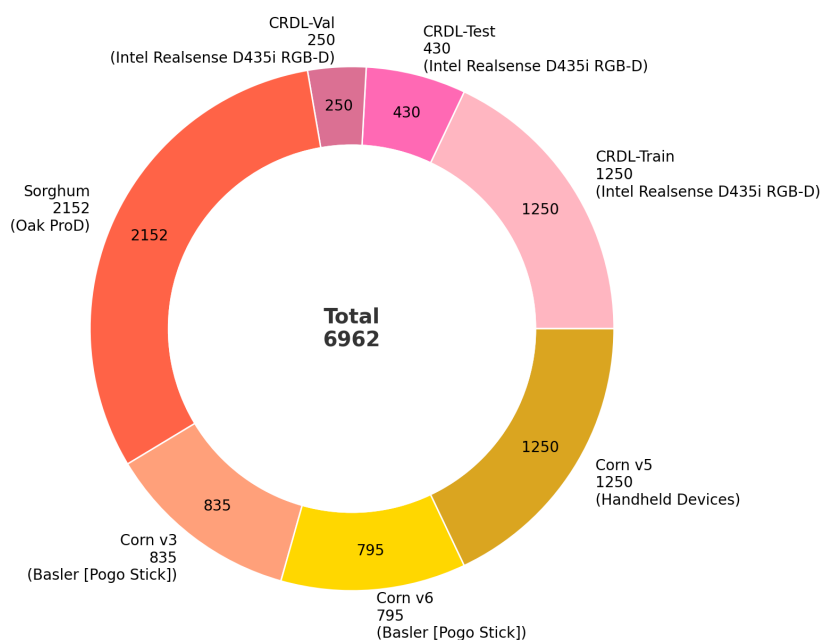


Figure 3: Distribution of image datasets used for row detection.

The complete dataset was then randomly divided into training, validation, and test subsets, with 64% allocated for training, 16% for validation, and 20% for testing.

2.1.3 Annotation

The Annotation process involved marking stalks for each plant using the polyline feature from [23]. In cases where the stalk was not visible, labelers were instructed to mark the boundary between the plant and the navigable path. Each row was represented as a polyline, with labelers required to mark at least four points per row to facilitate the fitting of second-degree polynomials. The labeled rows appear as blue curves in Figure 1. In the CRDL dataset, the boundary-based labeling method was adopted since stalks were not consistently visible.

2.1.4 Data Augmentation

To improve the model's robustness and ability to generalize across various conditions, a series of data augmentations were applied to the images. These augmentations introduced variations in scale, orientation, color, and other characteristics, effectively simulating a diverse range of real-world scenarios. The specific augmentations applied are as follows:

- **Random Affine Transformations:** Applied using *RandomAffine*, this transformation included rotation within -45 to 45 degrees, translation up to 20% along both axes, scaling between 0.8 and 1.5, and shear up to 30 degrees, with a probability of 0.5.
- **Weather Simulation:** Snow and rain effects were added with a probability of 0.5 each, simulating diverse weather conditions.
- **Color Jittering:** *ColorJitter* was used to introduce controlled variations in brightness (up to 0.5), contrast (up to 0.25), saturation (up to 0.05), and hue (up to 0.15), applied with a probability of 0.5.
- **Motion Blur:** Motion blur was implemented using *MotionBlur* with a kernel size of 5, an angle range of -0.5 to 0.5, and a direction range of -1 to 1, applied with a probability of 0.5.



Figure 4: Metering Stick

- **CutOut:** To enhance robustness against occlusions, *CutOut* was applied with a scale of $(0.1, 0.1)$, an aspect ratio between 0.3 and 0.5, and a probability of 0.5.
- **Random Horizontal Flip:** A random horizontal flip was applied with a probability of 0.25 using *RandomFlip*.

These augmentations introduced substantial variability into the training dataset, enhancing the model’s capacity to generalize effectively across a wide array of real-world conditions encountered in under-canopy row detection. All augmentations were implemented using the *kornia* Python library [24].

2.2 Predictions & Loss Functions

2.2.1 Predictions

Row Representation: Previous studies, such as [15, 16], represent predicted curves as polynomials of the form $v = f(u)$, where f is a polynomial of degree 3. Here, u corresponds to the horizontal image axis (width), and v corresponds to the vertical image axis (height). This representation has proven effective for lane detection, as lanes typically do not appear perpendicular to the vehicle’s direction of travel. In these scenarios, u remains continuous while v varies smoothly along the lane.

In contrast, agricultural row detection introduces scenarios where rows may appear perpendicular to the camera’s field of view, such as when the robot’s camera is oriented directly downward or when augmentations alter the row orientation. To address this, the current approach models both u and v as functions of a parameter λ . For a given set of n points, $[p_0, p_1, \dots, p_n]$, where each point is represented as $[u_i, v_i]$, the parameter λ_i is defined as:

$$\lambda_i = \frac{\sum_{j=1}^i \|p_{j-1}p_j\|}{\sum_{j=1}^n \|p_{j-1}p_j\|}, \quad (1)$$

where the numerator represents the cumulative distance from the starting point p_0 to the point p_i , and the denominator is the total cumulative distance across all points from p_0 to p_n . This param-

eterization ensures that predictions are independent of any specific axis, improving adaptability to diverse row orientations within the image.

To maintain consistency across images, the predicted u and v values are normalized relative to the image width and height, ensuring that the constant terms of the polynomial remain within the range $[0, 1]$. Consequently, the final row predictions are expressed as $U = f(\lambda)$ and $V = g(\lambda)$, where f and g are polynomials of degree k . This representation offers flexibility while maintaining consistency, enabling robust detection of rows across varying viewpoints.

Confidence: Given that the number of rows in an image can vary, each row prediction is accompanied by a confidence score to mitigate the risk of false positive detections. For a polynomial of degree k , the model outputs $2 \cdot (k + 1) + 1$ values for each row proposal. These include the coefficients for the u - and v -polynomials, along with an additional term representing the confidence score of the prediction.

2.2.2 Loss Functions

In this study, loss functions are employed to optimize alignment between the predicted and labeled curves in image space. Before applying polynomial fitting, the data points are sorted so that those closest to the camera are represented first. This preprocessing step ensures a consistent ordering along the curves U and V , which correspond to the horizontal and vertical components of the rows, respectively. Given the predictions \hat{U} and \hat{V} , several loss strategies are examined to minimize alignment error by comparing the polynomial coefficients directly. The methods include PolyOptLoss, Regression Loss, and Absolute Loss.

Regression Loss

Regression Loss minimizes the squared differences between the coefficients of the predicted and labeled polynomials. Given polynomial representations of the form:

$$U(\lambda) = \sum_{k=0}^n a_k \lambda^k \quad \text{and} \quad \hat{U}(\lambda) = \sum_{k=0}^n \hat{a}_k \lambda^k,$$

the Regression Loss for the predicted and labeled polynomials U and V can be expressed as:

$$\text{Regression Loss} = \sum_{k=0}^n \left((a_k - \hat{a}_k)^2 + (b_k - \hat{b}_k)^2 \right), \quad (2)$$

where a_k and b_k are the true polynomial coefficients, and \hat{a}_k and \hat{b}_k are the predicted coefficients for U and V , respectively. This loss function minimizes the squared error between polynomial coefficients, aiming to achieve close alignment across the entire curve.

Absolute Loss (L1 Loss)

Absolute Loss, or L_1 loss, minimizes the absolute differences between the coefficients of the predicted and labeled polynomials. Given the polynomial coefficients for the true and predicted curves, the Absolute Loss is defined as:

$$L_{abs} = \sum_{k=0}^n \left(|a_k - \hat{a}_k| + |b_k - \hat{b}_k| \right). \quad (3)$$

This loss function is less sensitive to large errors in individual coefficients, making it robust to variations and potentially outlier values in the polynomial representation.

PolyOptLoss

The proposed PolyOptLoss function minimizes the area between the predicted and labeled curves by evaluating the Euclidean distance at each parameterized point along the curve. For any point λ_i on the Row, the distance D_i between the predicted and labeled curves is calculated as:

$$D_i = \sqrt{(U(\lambda_i) - \hat{U}(\lambda_i))^2 + (V(\lambda_i) - \hat{V}(\lambda_i))^2}.$$

If interpreted as a potential energy in a spring-mass system, the energy at each point E_i considering the spring mass constant to be 1 is given by:

$$E_i = \frac{1}{2} \cdot D_i^2.$$

The total energy $T.E$ across the curve is then defined by integrating this energy over the curve parameter λ :

$$T.E = \int_0^1 E d\lambda. \quad (4)$$

PolyOptLoss minimizes this total energy, providing a cumulative measure of alignment between the predicted and labeled curves. By framing the alignment task as an energy minimization problem, PolyOptLoss is more Robust to labeling errors and adapts well to complex, curved structures in the field.

The PolyOptLoss function can be implemented in PyTorch as follows:

```

1 class PolyOptLoss(nn.Module):
2     def __init__(self, *args, **kwargs) -> None:
3         super().__init__(*args, **kwargs)
4
5     def forward(self, pred, target):
6         # Shapes for Hungarian Matcher
7         # pred shape [1, Predicted Polynomials, Axis, Degree+1]
8         # target shape [Target Polynomials, 1, Axis, Degree+1]
9         # Shapes for General Loss Function
10        # pred shape [Batch, Predicted Polynomials, Axis, Degree+1]
11        # target shape [Batch, Target Polynomials, Axis, Degree+1]
12        deg = pred.shape[-1] - 1
13        err = pred - target
14        factors = torch.arange(2*deg+1, deg, -1).view(-1, 1).to(err.device) -
15        ↪ torch.arange(deg+1).view(1, -1).to(err.device)
16        err_fac = (err.unsqueeze(-2) / factors.T).sum(dim=-1)
17        loss = torch.einsum("bpad, bpad -> bp", err_fac, err)
18        return loss

```

2.2.3 Matching & Total Loss

The total loss between a target row T and a predicted row P is expressed as:

$$L^{TP} = L_i^{TP} + L_c^{TP}$$

where: - L_i^{TP} denotes one of the alignment losses previously discussed (such as Regression Loss, Absolute Loss, or PolyOptLoss), which is applied directly to the polynomial coefficients. - L_c^{TP} represents the binary cross-entropy loss for classifying the Row as good detection.

Hungarian Matching Objective: Suppose there are N target rows and M predicted rows. The Hungarian matching algorithm aims to establish an optimal one-to-one correspondence $\sigma : \{1, \dots, N\} \rightarrow \{1, \dots, M\}$ that minimizes the cumulative loss for all matched pairs. The matching cost $\mathcal{C}(\sigma)$ is formulated as:

$$\mathcal{C}(\sigma) = \sum_{i=1}^N L^{T_{\sigma(i)} P_i} \quad (5)$$

where $\sigma(i)$ represents the assignment of target row $T_{\sigma(i)}$ to predicted row P_i , and $L^{T_{\sigma(i)}P_i}$ corresponds to the total loss L^{TP} for each paired match.

The objective of the Hungarian matcher is to find the permutation σ that minimizes the overall matching cost:

$$\sigma^* = \arg \min_{\sigma} \mathcal{C}(\sigma) = \arg \min_{\sigma} \sum_{i=1}^N \left(L_i^{TP} + L_c^{TP} \right)_{(T_{\sigma(i)}, P_i)} \quad (6)$$

Thus, σ^* denotes the optimal matching configuration that minimizes the combined alignment and classification losses across all target and predicted rows. This formulation allows for unique pairing between each target row and predicted row, effectively minimizing both alignment and classification discrepancies.

2.3 Architecture

This study employs two distinct architectures: one for evaluating the impact of different loss functions on polynomial proposals and another for the final comprehensive row detection model. For the loss analysis, a simpler architecture (described in Section 2.3.1) is used to isolate and examine the effects of Regression Loss and PolyOptLoss. For the final evaluation, a more sophisticated architecture is proposed (described in Section 2.3.2) to achieve robust row detection performance across varied conditions.

2.3.1 Loss Study (Architecture)

To investigate the effectiveness of different loss functions on polynomial proposal prediction, a streamlined architecture is introduced. The model architecture, illustrated in Figure 5, processes input images resized to 512x512 pixels through a backbone network, followed by additional processing layers for confidence scoring and polynomial coefficient prediction.

Backbone Network: The backbone extracts feature representations from the input images, and after testing multiple backbone networks, EfficientNet [25] emerged as the best-performing model, likely due to its use of Bidirectional Feature Pyramid Networks (Bi-FPNs) which enhance feature fusion across different scales. Other backbones, such as ResNet-18 [26] and RegNet [27], were also evaluated but did not perform as effectively in this configuration.

Feature Processing: After feature extraction by the backbone, a global average pooling (GAP) layer reduces the dimensionality, providing a condensed feature vector. This vector is then fed into three parallel Multi-Layer Perceptrons (MLPs), each dedicated to a specific prediction task:

- **Confidence Scores:** This MLP outputs confidence levels for each detected polynomial using a sigmoid activation function.
- **Polynomial Coefficients for U :** The second MLP predicts the coefficients for 10 polynomials representing the U component (horizontal alignment). It uses an Exponential Linear Unit (ELU) activation function in the first layer and a linear activation in the final layer for precise coefficient predictions.
- **Polynomial Coefficients for V :** The third MLP predicts the coefficients for 10 polynomials representing the V component (vertical alignment). Similar to the U MLP, this module uses an ELU activation in the first layer and a linear activation in the final layer.

This architecture enables a controlled analysis of the effect of different loss functions on polynomial proposal predictions without the added complexity of advanced transformers or attention mechanisms.

2.3.2 RowDetr (Architecture)

For the final evaluation, an architecture inspired by Rdetr [19] is implemented, as shown in Figure 7. This model utilizes a sophisticated encoder-decoder framework tailored for the challenges of row detection under dense canopy conditions. The architecture includes a backbone, hybrid encoder, polynomial proposal generation, PolySampler, offset network, and multi-scale deformable attention.

Backbone and Hybrid Encoder: Input images are first processed by a backbone network to extract high-level features. These features are then passed to a hybrid encoder, where self-attention is applied exclusively on the final layer. A top-down Feature Pyramid Network (FPN) is incorporated into the encoder to integrate multi-scale features, ensuring the detection of rows at varying resolutions and distances.

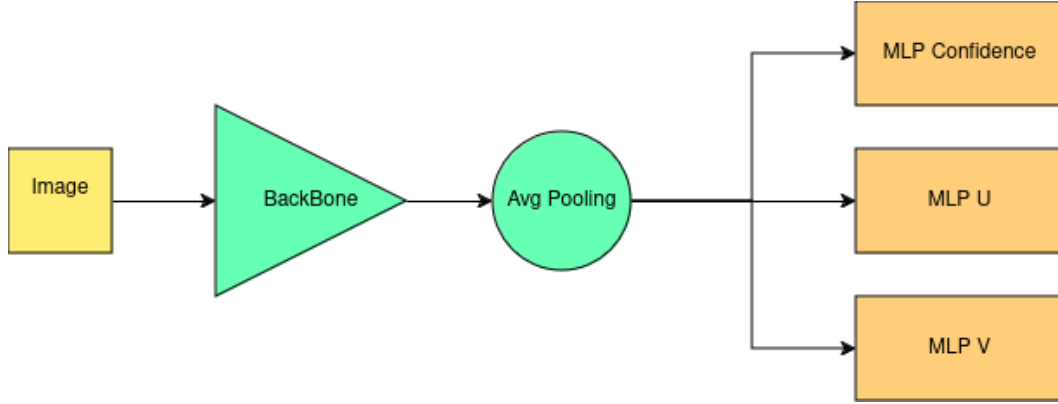


Figure 5: Model Architecture for Loss Study

Polynomial Proposals and Query Selection: From the encoded features, polynomial proposals are generated by selecting the top M queries from a logits head. Each query corresponds to a potential row in the image. These selected queries are then passed through an additional MLP head to predict the polynomial coefficients for the rows. Supervision is applied during this step to guide the logits head toward meaningful proposals. Gradients are detached during the proposal stage to ensure training stability and prevent noisy logits from destabilizing the learning process.

PolySampler and Offset Network: The selected polynomial proposals are further refined using the PolySampler module and an offset network. In the PolySampler module, sp points are sampled at equidistant values of λ , capturing structured features along the polynomial curves. Further these sampled points embeddings are obtained using a grid-based strategy at its respective feature level.

The offset network refines these sampled points to align them better with ground truth rows. It consists of a two-layer Multi-Layer Perceptron (MLP) with an output dimension of $2 \times np$, where np represents the number of resampling points. The final output of the MLP is adjusted using a scaled tanh activation function:

$$np = s \cdot \tanh(\text{MLP}(em)) + sp \quad (7)$$

where em represents the sampled embeddings, and s (0.035) is a small scaling factor.

Multi-Scale Deformable Attention: Refined proposals from the PolySampler and offset network are passed through a Multi-Scale Deformable Attention module [28]. This module attends to spatially relevant regions across multiple scales, effectively handling rows of varying shapes and sizes. The decoder uses these features to refine the polynomial predictions further, producing the final row detections.

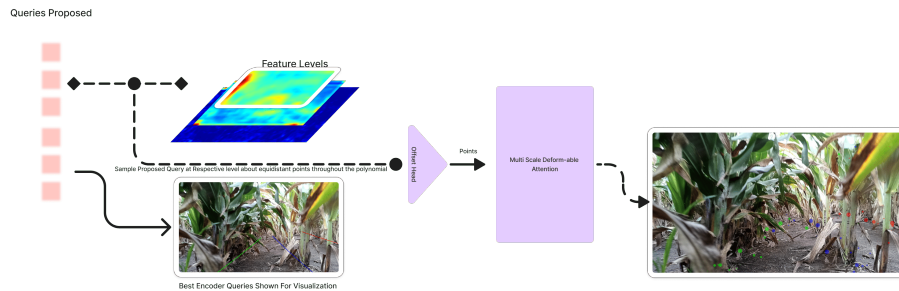


Figure 6: PolySampler Module: Sampling points across the encoder features. Larger points in the output indicate regions with higher attention scores.

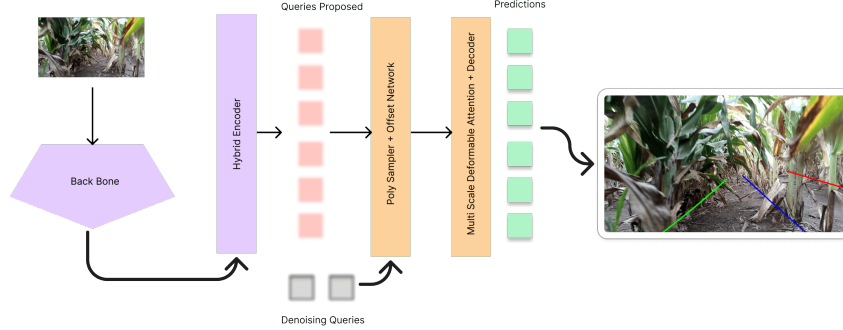


Figure 7: Model Architecture for RowDetr-Based Final Study

This RowDetr-based architecture, combining polynomial proposals, PolySampler, and deformable attention, provides a robust and efficient approach for row detection under dense canopy conditions. It eliminates the need for non-maximum suppression (NMS) [29] or other post-processing techniques, streamlining the detection pipeline.

3 Experiments

This section presents the experiments conducted, along with the metrics used for evaluation. In addition to the two primary studies, ablation studies were performed to analyze the contributions of individual components. Across all experiments, the target polynomials were restricted to 2-degree polynomials for consistency.

3.1 Evaluation Metrics

The evaluation of end-to-end row detection models currently depends on specific detection tasks, such as segmentation-based approaches [14] or line-detection metrics [18]. However, these approaches highlight the need for metrics that are adaptable across different detection methods. To address this, metrics such as TuSimple [30] and LPD [31] are adapted from lane detection metrics for evaluation and comparison of the final models. Additionally, for fairness and consistency, the metric provided by [18] is also utilized. The following subsections describe the evaluation metrics in detail.

1. **Mean Poly Distance (MPD):** MPD is a metric inspired by the PolyOptLoss function. It calculates the trapezoidal integral of the squared distance between predicted and ground truth polynomials, after matching predictions to targets based on minimum distance. Unmatched predictions (false positives) and missing targets (false negatives) incur a penalty corresponding to the maximum energy value (set to 2 in this case). The MPD is defined as:

$$MPD = \sum_{\lambda=0}^1 \left[(U(\lambda) - \hat{U}(\lambda))^2 + (V(\lambda) - \hat{V}(\lambda))^2 \right] \cdot 0.01, \quad (8)$$

where $U(\lambda)$ and $V(\lambda)$ represent the ground truth polynomials, and $\hat{U}(\lambda)$ and $\hat{V}(\lambda)$ represent the predicted polynomials.

2. **Accuracy Percent (AP):** Accuracy Percent measures the proportion of correct predictions relative to the total number of predictions. It is defined as:

$$AP = \frac{\text{Correct Predictions}}{\text{Total Predictions}}. \quad (9)$$

This metric provides a straightforward evaluation of the model’s accuracy in detecting rows.

3. **AgroNav F1 Metrics:** The F1 metrics proposed by [18] are based on the evaluation method introduced in [32]. In this approach, the ego lane is represented using two semantic lines spanning the

image. To adapt RowDetr’s predictions, polynomials are fitted to the ego lane, and two lines are extracted to match the input format required by AgroNav. The predictions are evaluated using the functions provided by [18], allowing for a direct comparison.

4. **TuSimple Metrics:** The TuSimple benchmark [30] evaluates performance using three key metrics: accuracy (Acc), false positive rate (FP), and false negative rate (FN). For a predicted row to be considered a true positive, its accuracy, defined as:

$$\text{Acc}(P_j, L_j^*) = \frac{1}{|L_j^*|} \sum_{(x_{i,j}^*, y_{i,j}^*) \in L_j^*} 1 [|p_j(y_{i,j}^*) - x_{i,j}^*| < \tau_{\text{acc}}], \quad (10)$$

must be greater than or equal to a predefined threshold ε . Here:

- L_j^* : Set of ground truth points for the j -th row.
- $(x_{i,j}^*, y_{i,j}^*)$: Ground truth coordinates.
- $p_j(y_{i,j}^*)$: Predicted x -coordinate for $y_{i,j}^*$.
- τ_{acc} : Maximum allowed deviation (20 pixels in TuSimple benchmark).
- ε : Accuracy threshold (set to 0.85).

The average values of Acc, FP, and FN are computed across all images, and the F1 scores are reported. This metric, however, can be sensitive to local errors as it considers all rows in the image, as noted by [33].

5. **Lane Position Deviation (LPD):** The LPD metric, introduced by [31], is adapted to emphasize the ego lane and to assign higher weight to the points closer to the camera. Ego lane is considered as the lane the robot is positioned in. In this context:

- The left boundary of the ego lane is the row closest to the center on the left.
- The right boundary is the row closest to the center on the robot’s right.

This metric quantifies the deviation of predicted rows from their expected positions relative to the robot’s perspective, providing a robust evaluation for row detection tasks.

3.2 Loss Study

3.2.1 Objective:

The primary objective of this study is to evaluate the impact of Regression Loss and PolyOptLoss on the performance of neural networks. Specifically, the study aims to understand how these loss functions influence learning when dealing with noisy labels in the sorghum dataset, which contains imperfections due to foliage and occlusions.

3.2.2 Experimental Setup:

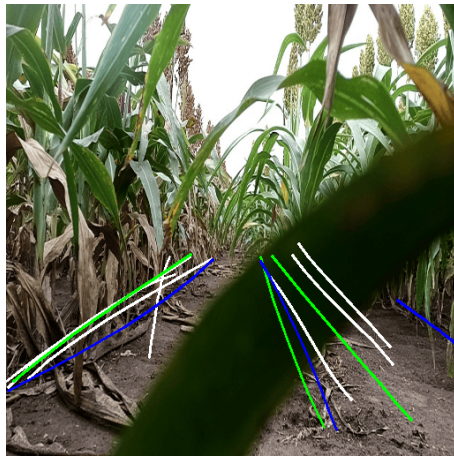
To investigate the effects of the loss functions, a subset of the sorghum dataset was selected. This subset included labels that were noisy and imperfect, allowing for a realistic assessment of how the networks handle challenging conditions. The models were trained for 300 epochs with the augmentations described in Section 2.1.4. Training was conducted on an Ubuntu 22.04 machine equipped with an NVIDIA RTX 4090 GPU, requiring approximately 4 hours per experiment. The backbones used for the models included EfficientNet_lite0, ResNet18, and RegNetX, as discussed in Section 2.3.1.

3.2.3 Results:

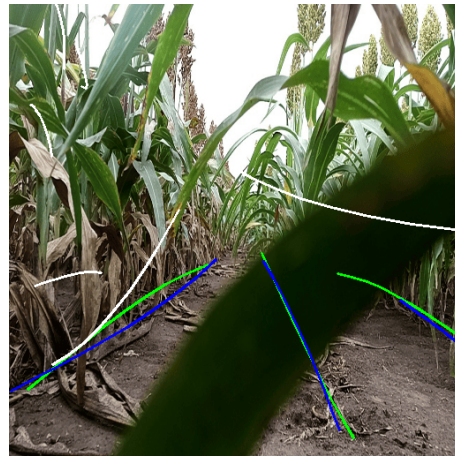
The Results are shown in the Table. 1, The accuracy percentage and MPD are reported for each of the backbones. To further explain the results some of the detections for Regression Loss and PolyOptLoss are shown in the Figure 8.

Back Bone	Loss	MPD	AP
EfficientNet	Regression	0.3862	0.73496
EfficientNet	PolyOptLoss	0.088	0.9835
RegNet	Regression	0.400	0.7678
RegNet	PolyOptLoss	0.097	0.9783
ResNet	Regression	0.769	0.7573
ResNet	PolyOptLoss	0.1289	0.9657

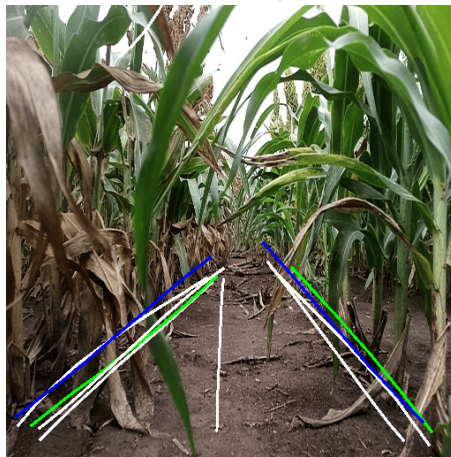
Table 1: Performance Metrics For Loss Study



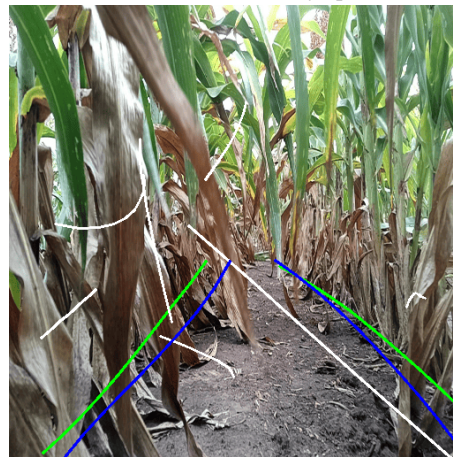
(a) Efficientnet with Regression Loss



(b) Efficientnet with PolyOptLoss



(c) Regnet with Regression Loss



(d) Regnet with PolyOptLoss

Figure 8: Detections of image in validationset
 White: Predictions with < 0.5 confidence; Blue: Labels; Green: Predictions with > 0.5 confidence

3.3 RowDetr

3.3.1 Objective:

The objective of this study is to evaluate the performance of the RowDetr architecture, described in Section 2.3.2, with different backbones. The results are compared against AgroNav [18], using the same evaluation metrics to ensure consistency.

3.3.2 Experimental Setup:

The complete dataset described in Section 2.1 was used to train both AgroNav and RowDetr. To align with AgroNav’s format, the polyline labels were converted by fitting straight lines to the ego lane. The ego lane is defined in Section 3.1. These fitted lines were extended across the entire image for compatibility with AgroNav’s input format.

For the RowDetr architecture, four feature levels were fed into the hybrid encoder, and the top three levels from the Feature Pyramid Network (FPN) were extracted for further processing. To compare how the reduction in levels compares with latency and accuracy, lowest latency model with three feature levels for the hybrid encoder and top three from FPN was also trained (regentx008-l-3).

AgroNav was trained until its F1-score plateaued, while RowDetr was trained for 500 epochs. For RowDetr 3 and 4 were utilized as total loss in 6. The training was conducted on the following system configuration:

- **Hardware:** Two NVIDIA RTX 4090 GPUs, AMD Ryzen Threadripper PRO 5955WX 16-Core Processor.
- **Software:** Python 3.8, PyTorch 2.1, MMEngine [34], and Ubuntu 22.04.

Training times varied, with AgroNav requiring approximately 8 hours and RowDetr completing in 6 hours. Despite handling more complex row detection scenarios, RowDetr demonstrated greater training efficiency compared to AgroNav.

3.3.3 Results:

The results are summarized in Table 2. AgroNav’s evaluation metrics, including F1-score (Mean F1), and Latency per prediction, were used for comparison. Parameter counts for each model are also reported to provide insights into their computational complexity.

To ensure a fair comparison, RowDetr’s predictions were converted into AgroNav’s format, as described in the Experimental Setup. This conversion allowed for a direct evaluation of the two models under identical criteria.

Model	Latency	Mean F1	Param Count
RowDetr(regentx008)	3.59 ms	0.9273	25M
RowDetr(regentx008)-l-3	2.05 ms	0.921	21M
RowDetr(resnet18)	3.73 ms	0.9270	30M
RowDetr(resnet50)	4.30 ms	0.9286	43M
RowDetr(efficientnet_lite0)	3.78 ms	0.92	21M
AgroNav	18 ms	0.8976	NA

Table 2: Comparison of different models for under-the-canopy navigation

4 Discussion

4.1 Loss Study

The results of the loss study, presented in Table 1 and Figure 8, illustrate the comparative performance of Regression Loss and PolyOptLoss across multiple backbone architectures. The findings clearly demonstrate the effectiveness of PolyOptLoss in addressing the challenges posed by noisy labels and occlusions in the sorghum dataset.

Quantitative Analysis: As shown in Table 1, models trained with PolyOptLoss consistently outperformed those trained with Regression Loss, achieving lower Mean Poly Distance (MPD) and higher Accuracy Percent (AP). Key observations include:

- With the EfficientNet backbone, MPD was significantly reduced from 0.3862 (Regression Loss) to 0.088 (PolyOptLoss), accompanied by an increase in AP from 0.73496 to 0.9835.

- The RegNet backbone also showed substantial improvements, with MPD decreasing from 0.400 to 0.097 and AP increasing from 0.7678 to 0.9783 when using PolyOptLoss.
- ResNet, while slightly lagging behind other backbones, demonstrated notable enhancements with PolyOptLoss, reducing MPD from 0.769 to 0.1289 and increasing AP from 0.7573 to 0.9657.

These results emphasize that PolyOptLoss consistently improves alignment between predictions and ground truth rows, even in the presence of noisy labels and occlusions.

Qualitative Analysis: The qualitative comparisons in Figure 8 further highlight the advantages of PolyOptLoss over Regression Loss. Notable observations include:

- Predictions from models trained with Regression Loss often showed a larger number of low-confidence predictions (white lines) concentrated near ground truth rows, which may be attributed to the noise in the dataset. These models struggled to consistently align predictions with labeled rows, as seen in Figures 8a and 8c.
- Models trained with PolyOptLoss generated more confident predictions (green lines) that closely followed ground truth rows (blue lines). Low-confidence predictions were more evenly distributed across the image, suggesting the model better generalizes to challenging scenarios, as shown in Figures 8b and 8d.
- PolyOptLoss-trained models maintained robust alignment even in regions with dense foliage or occlusions, showcasing their effectiveness in noisy environments. This is particularly evident in Figure 8b.

Comparison Across Backbones: Among the tested backbones, EfficientNet consistently delivered the best overall performance in terms of MPD and AP. This highlights the synergy between EfficientNet’s feature extraction capabilities and the geometric awareness introduced by PolyOptLoss. RegNet also performed competitively, while ResNet, despite showing improvements with PolyOptLoss, fell slightly behind in both metrics. These results suggest that the choice of backbone architecture plays a critical role in maximizing the effectiveness of PolyOptLoss.

Key Insights: The findings from this study underscore several important takeaways:

- PolyOptLoss is highly effective at minimizing alignment errors between predicted and ground truth rows by leveraging geometric information, providing a significant improvement over traditional Regression Loss.
- The improvements delivered by PolyOptLoss are consistent across different backbones, underscoring its generalizability and adaptability to various architectures.
- EfficientNet paired with PolyOptLoss emerged as the most robust and accurate configuration, making it particularly suitable for under-canopy navigation tasks where accuracy and reliability are critical.

4.2 RowDetr Study

The results presented in Table 2 and Figure 9 demonstrate the performance of the RowDetr architecture across different backbones compared to AgroNav [18]. These findings highlight RowDetr’s ability to deliver robust row detection with higher efficiency and accuracy.

Quantitative Analysis: As shown in Table 2, RowDetr consistently outperformed AgroNav across key metrics, including F1-score and latency:

- **Latency:** RowDetr exhibited significantly lower latency compared to AgroNav, achieving inference times as low as 3.47 ms (EfficientNet) and 3.59 ms (RegNetX-008), compared to AgroNav’s 18 ms. When optimized with TensorRT, latency was further reduced to 1.14 ms for RegNetX-008.
- **Mean F1-score:** RowDetr with the ResNet50 backbone achieved the highest F1-score of 0.9286, outperforming AgroNav’s score of 0.8976. Other backbones, such as RegNetX-008 and ResNet18, also demonstrated high F1-scores of 0.9273 and 0.9270, respectively.
- **Parameter Efficiency:** The EfficientNet_lite0 backbone demonstrated the smallest parameter count (21M), making it the most efficient configuration in terms of computational cost, while still achieving a competitive F1-score of 0.92.

These results emphasize that RowDetr not only provides higher accuracy but is also computationally more efficient than AgroNav, making it better suited for real-time under-canopy navigation.

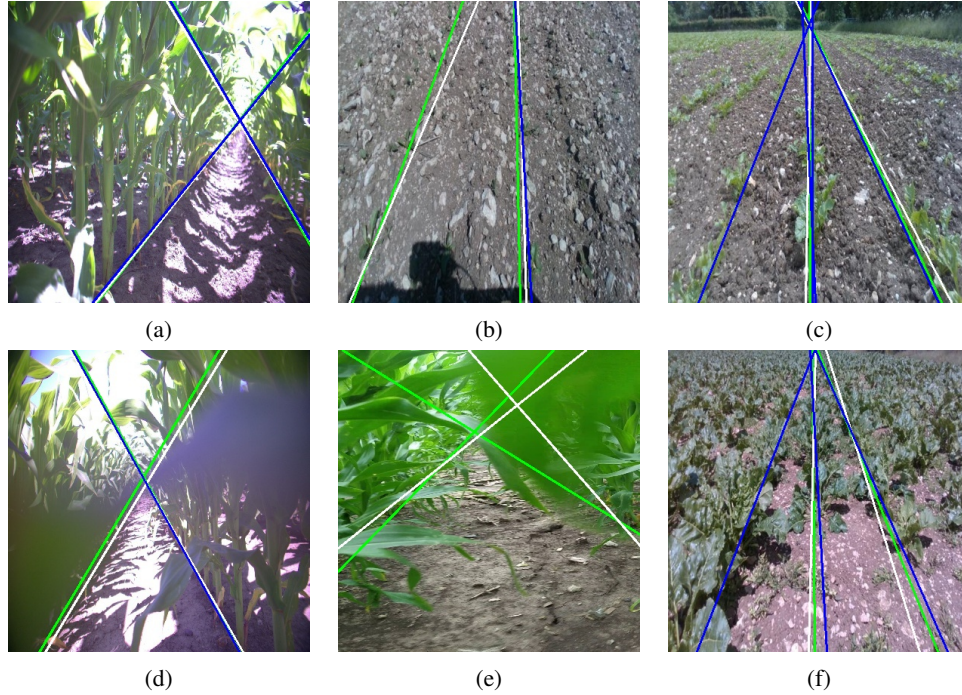


Figure 9: Detections on images in testset
 White:Labels; Blue: Agronav; Green: RowDetr Converted into agronav

Qualitative Analysis: The qualitative comparison in Figure 9 highlights the differences between RowDetr and AgroNav predictions. Key observations include:

- **Alignment with Ground Truth:** RowDetr’s predictions (green lines) align more closely with the ground truth (white lines) compared to AgroNav’s predictions (blue lines). This improved alignment is consistent across different scenarios, including rows partially occluded by foliage or shadows.
- **Handling Complex Scenarios:** In challenging conditions, such as dense vegetation (Figure 9d) or uneven lighting (Figure 9d), RowDetr maintained consistent and accurate predictions. AgroNav, on the other hand, showed occasional deviations and failed to align with certain row structures.
- **Robustness:** The robustness of RowDetr is further evident in its ability to generalize to different row geometries. Its predictions remained stable and accurate, even when rows varied in spacing or curvature. As these Rows being predicted are curves and RowDetr Does better representation compared to agronav as show in the Figure 9

Comparison Across Backbones: Among the tested backbones, ResNet50 delivered the highest accuracy, achieving an F1-score of 0.9286, making it the best choice for scenarios prioritizing precision. RegNetX-008 offered a strong balance between latency (3.59 ms) and accuracy (0.9273), making it suitable for real-time applications. EfficientNet_lite0, with the lowest parameter count (21M), demonstrated competitive performance while being computationally efficient, making it ideal for resource-constrained systems.

Key Insights: The results from this study underscore several important findings:

- **Performance:** RowDetr significantly outperforms AgroNav in both accuracy and efficiency, demonstrating its capability to handle complex row detection tasks.
- **BackBone Selection:** The choice of backbone influences the trade-off between accuracy, latency, and parameter efficiency, with ResNet50 excelling in precision and EfficientNet_lite0 providing computational efficiency and Regnet attaining the best of both the worlds.
- **Real-Time Capability:** With inference times as low as 3.57 ms (EfficientNet) and 1.14 ms (Regnet) when optimized with TensorRT, RowDetr is well-suited for real-time under-canopy navigation tasks.

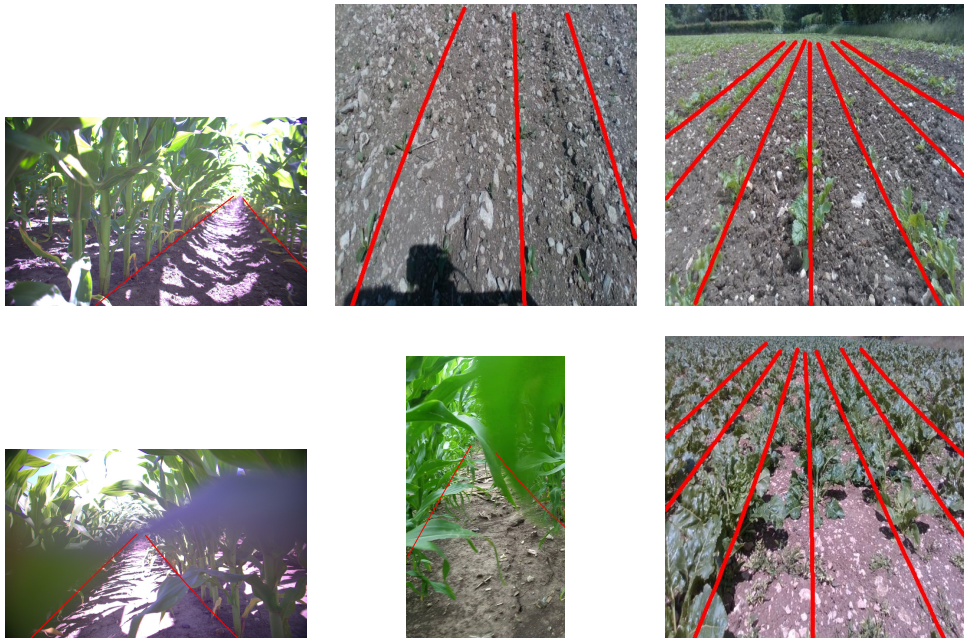


Figure 10: Detections on images in testset
Red: RowDet Predictions

4.3 Ablation Study:

4.3.1 Role of Encoder and Decoder in Row Detection

To begin, Figure 11 visualizes the polynomial proposals generated by the encoder and the refined detections from the decoder. The encoder’s predictions are shown on the left, while the decoder’s predictions are displayed on the right. Rows corresponding to the same proposal are represented in matching colors, with attention points visualized based on their attention scores, using the color of the respective row for consistency.

The encoder, lacking complete global context, occasionally produces proposals that deviate significantly from the correct row structures. For instance, in Figure 11a, the yellow proposal merges into the pink proposal. However, these errors are refined by the decoder through the use of polynomial proposals and the sampler network, as shown in Figure 11b.

Similarly, in Figures 11c and 11g, the blue row proposals incorrectly cross into the navigable path. After refinement in the decoder, these errors are corrected, as seen in Figures 11d and 11h. This highlights the decoder’s role in improving alignment and ensuring that predictions adhere to valid row structures.

4.3.2 Sampling Points and Offset Points

This section examines the influence of sampling points (sp) and offset points (np) on model performance. The polynomial degree is fixed at 2 across all experiments for consistent comparability. To avoid the smoothing effect of fitted curves, the analysis uses original labels from the labelers. The evaluation metrics include TuSimple Metrics—F1 score (higher is better), False Positive Rate (FPR, lower is better), and False Negative Rate (FNR, lower is better)—and the Lane Position Deviation (LPD) metric, which is crucial for assessing ego lane alignment (lower is better).

sp	np	LPD	TuSimple F1	TuSimple FNR	TuSimple FPR	Orin-AGX (int8) Latency (ms)
2	1	0.74049	0.8160	0.0473	0.2779	4.017
2	2	0.74723	0.7503	0.0618	0.3615	4.046
2	3	0.74270	0.8282	0.0347	0.2691	4.041
3	1	0.75288	0.8401	0.0412	0.2457	4.027
3	2	0.73384	0.8263	0.0338	0.2725	4.040
3	3	0.74125	0.8273	0.0475	0.2607	4.061
4	1	0.7516	0.8278	0.0382	0.2670	4.027
4	2	0.7544	0.8282	0.0414	0.2641	4.269
4	3	0.7504	0.8221	0.0416	0.2730	4.115

Table 3: Sampling Points and Offset Points Ablation Study

Quantitative Analysis: Table ?? highlights the interplay between sp and np , showcasing their effects on row detection accuracy, false positive/negative rates, and computational efficiency.

- **Effect of Sampling Points (sp):** Increasing sp improves the granularity of sampled embeddings, allowing better representation of the curve structure. For $sp = 3$ and $np = 2$, the model achieves the lowest LPD value (0.73384), indicating enhanced ego lane alignment. The highest TuSimple F1 score (0.8401) is achieved with $sp = 3$ and $np = 1$, alongside the lowest FPR (0.2457). However, further increasing sp to 4 yields diminishing returns, with slight degradation in both LPD and F1 scores. The optimal value of $sp = 3$ aligns with theoretical expectations for fitting a second-degree polynomial effectively, as three points are minimally required for accurate fitting.
- **Effect of Offset Points (np):** Offset points (np) determine the precision of adjustments applied to sampled embeddings. Increasing np from 1 to 2 significantly enhances performance. For example, at $sp = 3$, increasing np reduces the FNR from 0.0412 to 0.0338 and improves LPD. However, further increasing np to 3 leads to negligible improvements or slight degradation, as observed in the F1 score. This suggests $np = 2$ strikes an optimal balance between effective refinement and computational efficiency.
- **Combined Impact of sp and np :** The configuration $sp = 3$, $np = 2$ delivers the best performance, achieving the lowest LPD value (0.73384) and competitive TuSimple metrics. This combination ensures accurate row structure representation while minimizing prediction errors.
- **Latency Considerations:** All configurations achieve real-time performance, with latencies consistently below 4.3 ms on the Orin-AGX platform using int8 quantization. Notably, increasing np slightly impacts latency (+0.01 ms), while sp changes have minimal latency effects. This highlights the computational efficiency of the proposed approach.

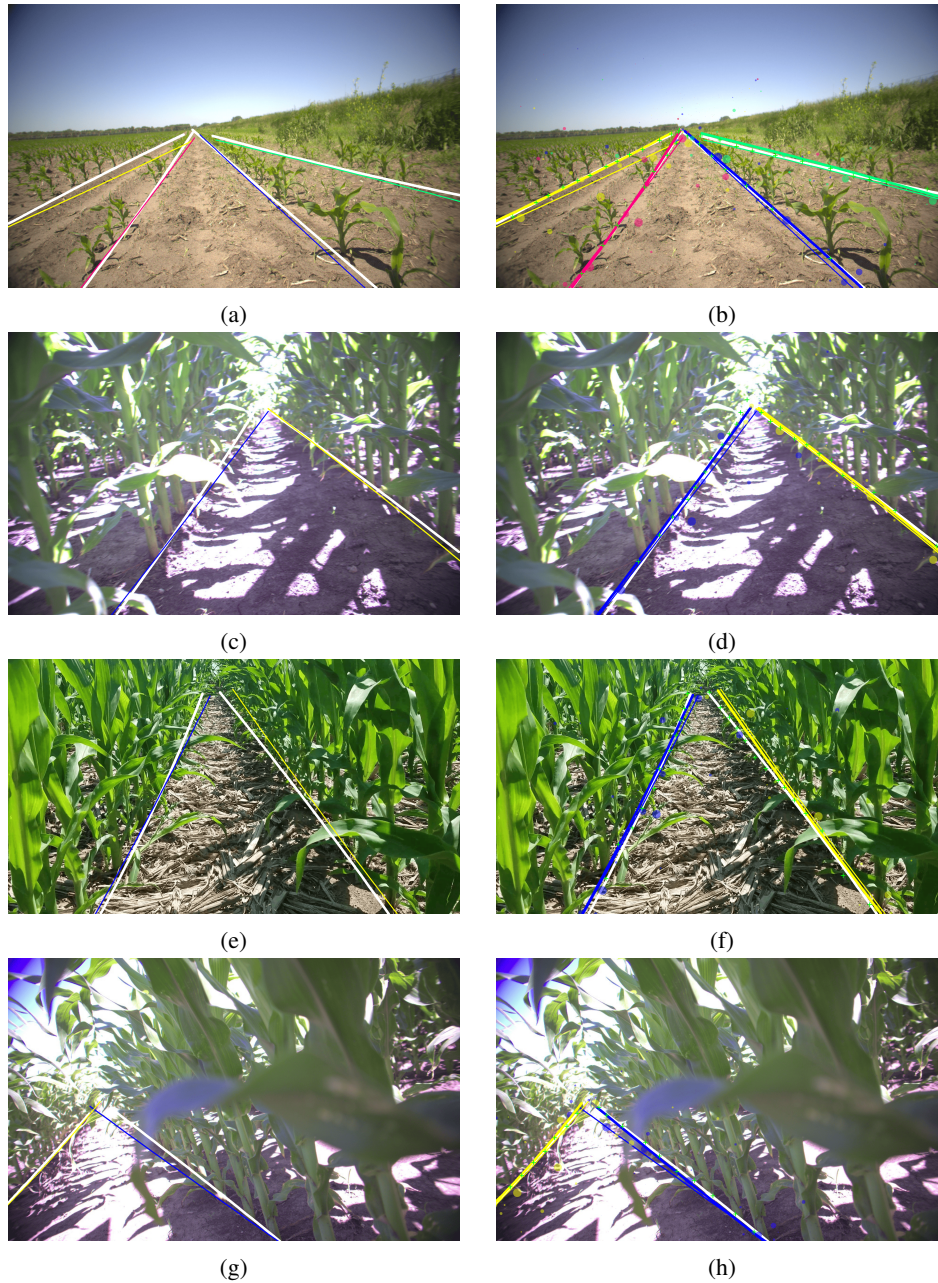


Figure 11: Encoder and Decoder Outputs on samples from validation set

Key Insights:

- Increasing sampling points (sp) enhances the model's ability to capture detailed row structures but exhibits diminishing returns beyond $sp = 3$.
- Offset points (np) refine predictions effectively, with $np = 2$ providing the best balance between accuracy and computational complexity.
- The optimal configuration ($sp = 3, np = 2$) offers the most reliable performance across metrics, making it ideal for under-canopy row detection tasks.
- The system maintains real-time efficiency across all configurations, with negligible latency increases from additional sampling or offset points.

Key Insights:

- Increasing sampling points (sp) improves the model’s ability to capture detailed row structures but exhibits diminishing returns beyond $sp = 3$, especially in the LPD metric.
- Offset points (np) effectively refine the sampled points, with $np = 2$ providing the best balance of performance and simplicity.
- The configuration $sp = 3, np = 2$ achieves the best overall performance, making it the most suitable choice for under-canopy row detection tasks.
- The system remains computationally efficient, achieving real-time performance across all configurations. One key insight is increasing np points in increasing in latency by 0.01ms where increasing sp is not impacting that drastically.

5 Conclusion

This study addresses the challenges of under-canopy navigation in dense agricultural environments by introducing a robust framework for row detection. The proposed contributions encompass key advancements in dataset curation, loss metric design, and model architecture, leading to significant improvements in performance and efficiency.

Key Findings:

- The introduction of the *PolyOptLoss* demonstrates a significant improvement over traditional loss functions like Regression Loss. By incorporating geometric information and minimizing alignment errors, PolyOptLoss consistently outperformed Regression Loss across multiple backbones, particularly in scenarios with noisy labels and occlusions.
- The proposed RowDetr architecture sets a new benchmark for row detection in dense and curved environments. Its ability to deliver high accuracy and robustness across a range of backbones underscores its flexibility and scalability. Furthermore, its compatibility with optimization techniques like TensorRT ensures low-latency performance, making it a practical solution for real-time agricultural applications.
- Ablation studies on sampling points and offset points reveal that optimal configurations ($sp = 3, np = 2$) provide the best balance between computational efficiency and detection accuracy. These findings highlight the importance of carefully tuning these parameters to maximize performance.
- Comparative evaluations against AgroNav demonstrate RowDetr’s superior performance across all metrics, including accuracy, false positive/negative rates, and latency. These results establish RowDetr as a state-of-the-art framework for end-to-end row detection tasks.

Impact and Future Work: The findings of this study lay a foundation for the development of more reliable and efficient autonomous systems tailored for agricultural applications. By addressing key limitations of existing methods, such as ensuring low latency and improving robustness to noisy environments, the proposed framework showcases its potential for deployment in real-world scenarios, including GPS-denied environments and dense crop fields.

Future work will aim to enhance the generalizability of the framework across a wider variety of crops and field conditions. The integration of multi-modal sensor data, such as LiDAR or thermal imaging, holds promise for improving performance in highly occluded environments. Moreover, leveraging self-supervised or semi-supervised learning techniques could reduce the reliance on large labeled datasets, thereby broadening the scope and practicality of the approach.

Additionally, navigation systems based on RowDetr detections will be developed and integrated with the framework, further extending its functionality and applicability in autonomous agricultural systems. These advancements will continue to refine the capabilities of under-canopy navigation, fostering progress in precision agriculture.

References

- [1] A. Atefi, Y. Ge, S. Pitla, and J. Schnable. Robotic technologies for high-throughput plant phenotyping: Contemporary reviews and future perspectives. *Front. Plant Sci.*, 12:611940, June 2021.
- [2] R. Rahmadian and M. Widartono. Autonomous robotic in agriculture: A review. In *2020 Third International Conference on Vocational Education and Electrical Engineering (ICVEE)*, pages 1–6, 2020. doi:10.1109/ICVEE50212.2020.9243253.
- [3] M. Kise, N. Noguchi, K. Ishii, and H. Terao. Enhancement of turning accuracy by path planning for robot tractor. In *Automation Technology for Off-Road Equipment Proceedings of the 2002 Conference*, page 398. American Society of Agricultural and Biological Engineers, 2002.
- [4] S. Gan-Mor, R. L. Clark, and B. L. Upchurch. Implement lateral position accuracy under rtk-gps tractor guidance. *Computers and Electronics in Agriculture*, 59(1-2):31–38, 2007.
- [5] B. Yan, G. Wu, Y. Xiao, H. Mei, and Z. Meng. Development and evaluation of a seed position mapping system. *Computers and Electronics in Agriculture*, 190:106446, 2021. ISSN 0168-1699. doi:<https://doi.org/10.1016/j.compag.2021.106446>. URL <https://www.sciencedirect.com/science/article/pii/S0168169921004634>.
- [6] R. H. Cheppally, A. Sharda, and G. Wang. Seed localization system suite with cnns for seed spacing estimation, population estimation and doubles identification. *Smart Agricultural Technology*, 4:100182, 2023. ISSN 2772-3755. doi:<https://doi.org/10.1016/j.atech.2023.100182>. URL <https://www.sciencedirect.com/science/article/pii/S2772375523000126>.
- [7] T. Mueller-Sim, M. Jenkins, J. Abel, and G. Kantor. The robotanist: A ground-based agricultural robot for high-throughput crop phenotyping. In *2017 IEEE International Conference on Robotics and Automation (ICRA)*, pages 3634–3639, 2017. doi:10.1109/ICRA.2017.7989418.
- [8] E. S. Calera, G. C. d. Oliveira, G. L. Araujo, J. I. F. Filho, L. Toschi, A. C. Hernandez, A. E. B. Velasquez, M. V. Gasparino, G. Chowdhary, V. A. H. Higuti, and M. Becker. Under-canopy navigation for an agricultural rover based on image data. *Journal of intelligent & robotic systems.*, 108(2), 2023-06. ISSN 0921-0296.
- [9] A. Sivakumar, S. Modi, M. Gasparino, C. Ellis, A. Baquero Velasquez, G. Chowdhary, and S. Gupta. Learned visual navigation for under-canopy agricultural robots. In *Robotics: Science and Systems XVII, RSS2021*. Robotics: Science and Systems Foundation, July 2021. doi:10.15607/rss.2021.xvii.019. URL <http://dx.doi.org/10.15607/RSS.2021.XVII.019>.
- [10] A. N. Sivakumar, M. V. Gasparino, M. McGuire, V. A. H. Higuti, M. U. Akcal, and G. Chowdhary. Lessons from deploying cropfollow++: Under-canopy agricultural navigation with keypoints, 2024.
- [11] D. Li, B. Li, S. Kang, H. Feng, S. Long, and J. Wang. E2cropdet: An efficient end-to-end solution to crop row detection. *Expert Systems with Applications*, 227:120345, 2023. ISSN 0957-4174. doi:<https://doi.org/10.1016/j.eswa.2023.120345>. URL <https://www.sciencedirect.com/science/article/pii/S0957417423008473>.
- [12] Y. Yang, Y. Zhou, X. Yue, G. Zhang, X. Wen, B. Ma, L. Xu, and L. Chen. Real-time detection of crop rows in maize fields based on autonomous extraction of roi. *Expert Systems with Applications*, 213:118826, 2023.
- [13] J. Yu, J. Zhang, A. Shu, Y. Chen, J. Chen, Y. Yang, W. Tang, and Y. Zhang. Study of convolutional neural network-based semantic segmentation methods on edge intelligence devices for field agricultural robot navigation line extraction. *Computers and Electronics in Agriculture*, 209:107811, 2023. ISSN 0168-1699. doi:<https://doi.org/10.1016/j.compag.2023.107811>. URL <https://www.sciencedirect.com/science/article/pii/S0168169923001990>.
- [14] R. de Silva, G. Cielniak, G. Wang, and J. Gao. Deep learning-based crop row detection for infield navigation of agri-robots. *Journal of Field Robotics*, n/a(n/a). doi:<https://doi.org/10.1002/rob.22238>. URL <https://onlinelibrary.wiley.com/doi/abs/10.1002/rob.22238>.
- [15] C. Yang, Z. Tian, X. You, K. Jia, T. Liu, Z. Pan, and V. John. Polylandenet++: enhancing the polynomial regression lane detection based on spatio-temporal fusion. *Signal, Image and Video Processing*, pages 1–10, 2024.
- [16] L. Tabelini, R. Berriel, T. M. Paixão, C. Badue, A. F. D. Souza, and T. Oliveira-Santos. Polylandenet: Lane estimation via deep polynomial regression, 2020.

- [17] X. Li, Z. Huang, X. Sun, and T. Liu. A fast detection method for polynomial fitting lane with self-attention module added. In *2021 International Conference on Control, Automation and Information Sciences (ICCAIS)*, pages 46–51, 2021. doi:10.1109/ICCAIS52680.2021.9624545.
- [18] S. K. Panda, Y. Lee, and M. K. Jawed. Agronav: Autonomous navigation framework for agricultural robots and vehicles using semantic segmentation and semantic line detection, 2023. URL <https://arxiv.org/abs/2304.04333>.
- [19] Y. Zhao, W. Lv, S. Xu, J. Wei, G. Wang, Q. Dang, Y. Liu, and J. Chen. Detsr beat yolos on real-time object detection, 2024. URL <https://arxiv.org/abs/2304.08069>.
- [20] 2022. URL <https://www.nvidia.com/content/dam/en-zz/Solutions/gtcf21/jetson-orin/nvidia-jetson-agx-orin-technical-brief.pdf>.
- [21] The4. Oak-d pro. URL <https://shop.luxonis.com/products/oak-d-pro>.
- [22] S. Macenski, T. Foote, B. Gerkey, C. Lalancette, and W. Woodall. Robot operating system 2: Design, architecture, and uses in the wild. *Science Robotics*, 7(66):eabm6074, 2022. doi:10.1126/scirobotics.abm6074. URL <https://www.science.org/doi/abs/10.1126/scirobotics.abm6074>.
- [23] Labelbox. Labelbox. <https://labelbox.com>, 2024. Online.
- [24] E. Riba, D. Mishkin, D. Ponsa, E. Rublee, and G. Bradski. Kornia: an open source differentiable computer vision library for pytorch. In *Winter Conference on Applications of Computer Vision*, 2020. URL <https://arxiv.org/pdf/1910.02190.pdf>.
- [25] M. Tan and Q. Le. Efficientnet: Rethinking model scaling for convolutional neural networks. In *International conference on machine learning*, pages 6105–6114. PMLR, 2019.
- [26] S. Targ, D. Almeida, and K. Lyman. Resnet in resnet: Generalizing residual architectures. *arXiv preprint arXiv:1603.08029*, 2016.
- [27] J. Xu, Y. Pan, X. Pan, S. Hoi, Z. Yi, and Z. Xu. Regnet: self-regulated network for image classification. *IEEE Transactions on Neural Networks and Learning Systems*, 2022.
- [28] X. Zhu, W. Su, L. Lu, B. Li, X. Wang, and J. Dai. Deformable detr: Deformable transformers for end-to-end object detection, 2021. URL <https://arxiv.org/abs/2010.04159>.
- [29] P. Sun, Y. Jiang, E. Xie, W. Shao, Z. Yuan, C. Wang, and P. Luo. What makes for end-to-end object detection?, 2021.
- [30] Tusimple lane detection challenge. https://github.com/TuSimple/tusimple-benchmark/tree/master/doc/lane_detection, 2017. Accessed: 2024-11-14.
- [31] R. K. Satzoda and M. M. Trivedi. On performance evaluation metrics for lane estimation. In *2014 22nd International Conference on Pattern Recognition*, pages 2625–2630, 2014. doi:10.1109/ICPR.2014.453.
- [32] K. Zhao, Q. Han, C.-B. Zhang, J. Xu, and M.-M. Cheng. Deep hough transform for semantic line detection. *IEEE Transactions on Pattern Analysis and Machine Intelligence*, page 1–1, 2021. ISSN 1939-3539. doi:10.1109/tpami.2021.3077129. URL <http://dx.doi.org/10.1109/TPAMI.2021.3077129>.
- [33] T. Sato and Q. A. Chen. Towards driving-oriented metric for lane detection models, 2022. URL <https://arxiv.org/abs/2203.16851>.
- [34] M. Contributors. MMEngine: Openmmlab foundational library for training deep learning models. 2022.